Measurement of the Absolute np Scattering Differential Cross Section at 194 MeV

M. Sarsour,[1] T. Peterson,[1,*] M. Planinic,[1,†] S. E. Vigdor,[1] C. Allgower,[1] B. Bergenwall,[2] J. Blomgren,[2] T. Hossbach,[1] W. W. Jacobs,[1] C. Johansson,[2] J. Klug,[2] A. V. Klyachko,[1] P. Nadel-Turonski,[2] L. Nilsson,[2] N. Olsson,[2] S. Pomp,[2] J. Rapaport,[3] T. Rinckel,[1] E. J. Stephenson,[1] U. Tippawan,[2,4] S. W. Wissink,[1] and Y. Zhou[1]

[1]*Indiana University Cyclotron Facility and Department of Physics, Bloomington, Indiana 47408, USA*
[2]*Uppsala University, Uppsala, Sweden*
[3]*Ohio University, Athens, Ohio, USA*
[4]*Chiang Mai University, Chiang Mai, Thailand*

(Received 11 December 2004; published 3 March 2005)

We describe a double-scattering experiment with a novel tagged neutron beam to measure differential cross sections for np backscattering to better than $\pm 2\%$ absolute precision. The measurement focuses on angles and energies where the cross section magnitude and angle dependence constrain the charged pion-nucleon coupling constant, but existing data show serious discrepancies among themselves and with energy-dependent partial-wave analyses. The present results are in good accord with the partial-wave analyses, but deviate systematically from other recent measurements.

DOI: 10.1103/PhysRevLett.94.082303 PACS numbers: 25.40.Dn, 13.75.Gx, 25.10.+s, 28.20.Cz

The neutron-proton elastic scattering database at intermediate energies is plagued by experimental inconsistencies and cross section normalization difficulties [1–3]. These problems have led the most sophisticated partial-wave analyses (PWAs) of the data [4–6] to ignore the majority (including the most recent) of measured cross sections, while the literature is filled with heated debates over experimental and theoretical methods [7,8], including proposed radical ''doctoring'' (angle-dependent renormalization) to ''salvage'' allegedly flawed data [9]. Meanwhile, an empirical evaluation of a fundamental parameter of meson-exchange theories of the nuclear force—the charged πNN coupling constant f_c^2—hangs in the balance [8]. We report here the results of a new experiment, carried out utilizing quite different techniques from earlier measurements in an attempt to resolve the most worrisome experimental discrepancies.

The present experiment involves a kinematically complete double-scattering measurement to produce and utilize a ''tagged'' intermediate-energy neutron beam [10], thus greatly reducing the usual systematic uncertainties associated with the determination of neutron flux. Products from the second scattering were detected over the full angle range of interest simultaneously in a large-acceptance detector array, to eliminate the need for cross normalization of different regions of the angular distribution. The use of carefully matched solid CH_2 and C targets permitted frequent measurement and accurate subtraction of quasi-free scattering background, thereby minimizing reliance on kinematic cuts to isolate the free np scattering sample. These methods, combined with multiple internal cross-checks built into the data analysis procedures, have allowed us to achieve systematic error levels in the absolute cross section below 2%. In addition to addressing the previous discrepancies, the results provide a useful absolute cross section calibration for intermediate-energy neutron-induced reactions.

The experiment was carried out during the final year of operation of the Indiana University Cyclotron Facility's Cooler ring [11], with apparatus illustrated in Fig. 1 and described in detail in [10]. Neutrons of 185–197 MeV were produced via the charge-exchange reaction $p + d \rightarrow n + 2p$, initiated by a stored, electron-cooled 203 MeV proton beam, with typical circulating current of 1–2 mA, in a windowless deuterium gas jet target (GJT) of thickness ≈ 2–4×10^{15} atoms/cm^2. The ultrathin target permitted detection of the two low-energy recoil protons in an array (''tagger'' in Fig. 1) of four 6.4×6.4 cm^2 double-sided silicon strip detectors (DSSD's) with 480 μm readout pitch in two orthogonal directions, each followed by a silicon pad (''backing'') detector (BD) of the same area. Only recoil protons ($\lesssim 11$ MeV) that stopped in either the DSSD's or BD's were considered in the data analysis. Measurements of energy, arrival time, and two-dimensional position for both recoil protons in the tagger, when combined with precise knowledge of cooled p beam direction and energy, allowed four-momentum determination for each produced neutron on an event-by-event basis.

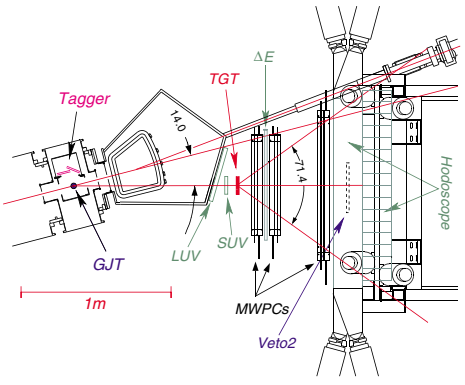

FIG. 1 (color online). Top view of the np scattering experiment setup.

The (uncollimated) tagged neutrons were distributed over a significant range in energy and angle, but these parameters were measured for each produced neutron with resolutions $\sigma_E \approx 60$ keV and $\sigma_{\text{angle}} \approx 2$ mrad.

The forward setup included a solid secondary scattering target of CH_2 or graphite positioned 1.1 m downstream of the GJT, centered on a neutron production laboratory angle of 14.0°. Both solid targets had transverse dimensions 20×20 cm^2 and thickness of 0.99×10^{23} carbon atoms/cm^2. The typical rate of tagged neutrons with energy above 185 MeV intercepting the secondary target was 200 s^{-1}. A large and a small upstream veto scintillator (LUV and SUV, respectively, in Fig. 1) vetoed tagged neutrons that interacted before the secondary target. Following the target was a forward array of plastic scintillators for triggering and energy information and a set of three (three-plane) multiwire proportional chambers (MWPC's) to track forward protons. The forward detector acceptance was nearly 100% for np scattering events with $\theta_{\text{c.m.}} \geq 130°$, falling to 50% by $\theta_{\text{c.m.}} = 90°$. The MWPC between the secondary target and ΔE scintillator allowed discrimination against np events initiated in that scintillator. The rear hodoscope comprised 20 plastic scintillator bars of sufficient thickness (20 cm) to stop 200 MeV protons and give 15–20% detection efficiency for 100–200 MeV neutrons.

Specially designed DSSD front-end electronics [10] permitted a tagger-based event trigger on neutron candidates (consistent with two distinct tagger hits and no accompanying signals from LUV or SUV), whether or not the neutrons interacted in the forward target and/or detectors. Tagged neutron events were recorded in three mutually exclusive event streams [10], coupling the tagger trigger with (1) no rear hodoscope coincidence (providing a prescaled sample for neutron flux monitoring); or (2) a coincidence with both the ΔE scintillator and rear hodoscope (for np scattering candidates); or (3) a coincidence with the rear hodoscope but not ΔE (for evaluating the neutron detection efficiency of the hodoscope). Comparative analyses of the three separate event streams, with respective yields N_1, N_2, and N_3, facilitated crosschecks to calibrate the system [10] and to study potential systematic errors.

Neutron beam properties were defined by identical cuts for all three event streams, so that associated systematic uncertainties would cancel in the yield ratios from which the absolute np scattering cross section is extracted. Among the common cuts are ones on DSSD vs BD energy deposition in the tagger [10], used to select two tagged neutron classes for analysis: (a) "2-stop" events, where both recoil protons stopped inside the DSSD's (either the same or different quadrants of the tagger); (b) "1-punch" events, where one of two recoil protons incident on different quadrants punched through into the corresponding BD and stopped there. These classes differ significantly in neutron energy (E_n) and position profiles [10], allowing an important crosscheck on the accuracy of the tagging technique by comparing np cross sections extracted independently from each class. Other common cuts defined a fiducial area for neutrons impinging on the secondary target and eliminated common-mode BD noise (via pulse-height correlations among quadrants) that sometimes led to misidentification of event class.

Additional misidentification discovered during data analysis was attributed to an electronics malfunction in the gating or clearing circuit for one analog-to-digital converter module, that removed all valid BD energy signals for some fraction of events. The corrupted events were misidentified as 2-stop events, with systematically incorrect predictions of tagged neutron trajectory (since some recoil proton energy was missed), and hence of np scattering angle for event stream 2. A subsample of these corrupted events could be isolated by means of their valid BD timing signals, and their properties were accurately reproduced by appropriately scaling the surviving sample of all events with valid BD energies and times, after setting these energies to zero in software. Thus, the surviving punch-through events permitted a reliably unbiased subtraction of the corrupted 2-stop events, independently for each event stream. The subtraction confirmed that the same fraction (typically 23%) of punch-through events was lost from each event stream, with no net effect on the extracted 1-punch cross sections.

Kinematic cuts applied exclusively to event stream 2 to define np free-scattering events from the secondary target were used sparingly. We relied instead on accurate background subtraction facilitated by frequent interchange of the carefully matched CH_2 and C targets. The CH_2 and C runs were normalized via the pd elastic scattering yield from the GJT measured in a fourth event stream for the two targets. The pd events were identified by their clear kinematic locus in the energy of recoil deuterons detected in the tagger *vs* the position of coincident forward protons in the front MWPC. The subtraction removed not only quasifree scattering off carbon nuclei in the target, but also background from other sources, such as tagged n scattering from the aluminum support platform on which the secondary target sat, or protons produced in the GJT that passed above the top of the LUV and SUV scintillators, mocking up np backscattering events.

The success of the background subtraction is illustrated in Fig. 2, where 2(a) and 2(b) show the vertical position

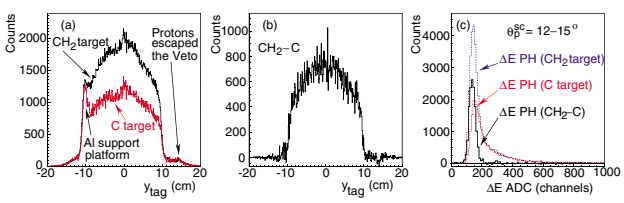

FIG. 2 (color online). Distributions of np scattering candidate events in y_{tag} (a), (b) and ΔE (c) for CH_2 and C targets and their difference.

($y_{\rm tag}$) of neutrons on the secondary target, as reconstructed from the tagger, for CH_2 and normalized C targets, and for their difference. Figure 2(c) shows the ΔE pulse-height spectrum within a given scattering angle (θ_p^{sc}) bin for both targets and for their difference. Prominent background features associated both with the secondary target (e.g., the long quasifree scattering tail in ΔE) and with other sources [e.g., the peak in frame (a) from the Al support platform] are simultaneously accurately removed by the subtraction. The subtraction reveals in frame (b) a $y_{\rm tag}$ distribution reflecting the tagged n (2-stop + 1-punch) beam profile, convoluted with the np scattering cross section, forward detector acceptance and sharp CH_2 target edges (the sharpness illustrating the good spatial resolution of the tagging).

Background-subtracted spectra such as that in Fig. 2(c) were used to evaluate efficiencies for the few loose cuts imposed on event stream 2 to improve the free-scattering signal-to-background ratio, including ones on ΔE *vs* θ_p^{sc} and on MWPC proton track quality. Cuts on the hodoscope pulse height were avoided, to remove reliance on detailed understanding of the nuclear reaction tail for protons stopping in this thick scintillator.

The forward detector acceptance was determined as a function of θ_p^{sc} from simulations matched to *measured* distributions of np free-scattering events in proton azimuthal angle ϕ_p. In the simulations, the longitudinal coordinate of the n production vertex within the GJT and its transverse coordinates on the secondary target were generated randomly for each event, but within distributions determined from the experiment. These coordinates determined the incident n angle. Generated outgoing p trajectories were accepted if they produced signals above the hodoscope threshold (required in the trigger) and in all three MWPCs (required in the data analysis). Forward

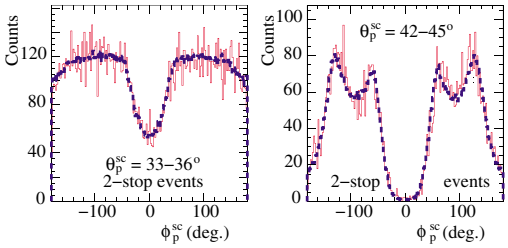

FIG. 3 (color online). The distribution of free (CH_2-C) np scattering events with respect to proton azimuthal angle ϕ, for two laboratory scattering angle bins. The solid (dashed) histograms are measured (simulated and normalized to fit the measurements).

detector location parameters were tuned to reproduce the measured ϕ_p distributions for all θ_p^{sc} bins and for 1-punch and 2-stop samples simultaneously. Typical fits in Fig. 3 reveal a structure of purely geometric origin, from rectangular detector edges projected on θ and ϕ. For $\theta_p^{sc} \leq 24°$ the measured and simulated ϕ distributions are uniform, since the scattered protons are completely contained within the forward array.

Absolute differential cross sections were obtained from the yields in event streams 1, 2, and 3 defined above:

$$\left(\frac{d\sigma}{d\Omega}\right)_{\rm lab} = \frac{N_2(\theta_p^{sc}) \prod c_i}{(N_1 + N_2 + N_3) t_H |d\cos(\theta_p^{sc})| a_\phi(\theta_p^{sc})}, \quad (1)$$

where N_j represents the number of events (corrected for prescaling where appropriate) surviving all relevant cuts and background subtractions for event stream j; the c_i are small corrections, summarized in Table I, for inefficiencies, tagged neutron losses or backgrounds, and software cut and dead time differences among event streams; $t_H = (1.988 \pm 0.008) \times 10^{23}$ H atoms/cm^2 for the CH_2

TABLE I. Correction factors (c_i) and systematic uncertainties in correction factors for the np cross sections.

Source	Correction factor	Uncertainty
Accidental tagger coincidences	1.0003	$< \pm 0.001$
Non-D_2 tagger background	1.0067 (2-stop); 1.0044 (1-punch)	± 0.002
n position uncertainty on CH_2	1.0000	± 0.001
n attenuation before CH_2	1.005	± 0.0025
C background subtraction	1.0000	± 0.004
Reaction tail losses	1.004	± 0.002
Neutron polarization effects	Angle dependent: >0.9988 (1-punch); <1.0014 (2-stop)	± 0.001
Software cut losses	1.010	± 0.005
Sequential reactions and $x_{\rm tag}(n)$ errors	1.063	± 0.010
CH_2 target thickness	1.0000	± 0.004
np scattering acceptance	1.0000	$\leq \pm 0.001$ ($>120°$) $\rightarrow \pm 0.017$ (90°)
MWPC inefficiency	1.017	± 0.002
Trigger inefficiency	$1.002 + 0.008 \times \cos^2(\theta_p^{\rm LAB})$	$\pm[0.001 + 0.004 \times \cos^2(\theta_p^{\rm LAB})]$
Dead time differences	0.991	± 0.005
Scattering angle errors	1.000	angle dependent, $\leq \pm 0.004$
Corruption subtraction	1.000	$< \pm 0.001$
Net	≈ 1.10	$\approx \pm 0.015$

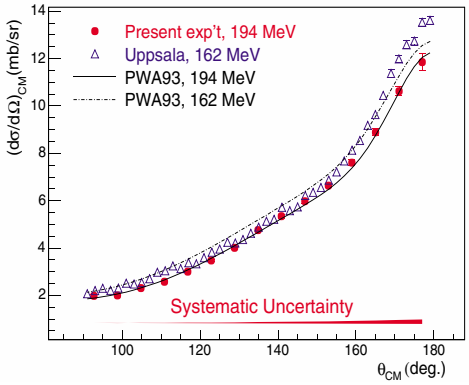

FIG. 4 (color online). Absolute differential cross section from the present experiment, compared with data from Ref. [3] and with PWA calculations at two relevant energies. The error bars and shaded band for the present results represent, respectively, statistical (including background subtraction) and systematic (including overall normalization) uncertainties.

target; and a_ϕ is the azimuthal acceptance determined from simulations for the given angle bin. The data were analyzed in 1 MeV wide E_n slices from 185 to 197 MeV. An effective cross section at $\langle E_n \rangle = 194.0 \pm 0.15$ MeV was extracted by applying small (always $<1\%$) corrections to the results for each E_n slice, based on the energy dependence calculated with the Nijmegen PWA [4].

Cross sections extracted independently for the 1-punch and 2-stop samples agree within statistical uncertainties (χ^2/point ≈ 1.0) in both magnitude and angular shape. This comparison supports the reliability of the experiment and analysis, as these events come from complementary regions of the tagged beam spatial and energy profiles [10]. Cross sections extracted for different time periods within the production runs, and with different sets of cuts, are also consistent within the uncertainties. The results, averaged over the 2-stop and 1-punch samples, are compared in Fig. 4 with previous experimental results at 162 MeV [3] and with the Nijmegen partial-wave analysis (PWA93) at the two relevant energies [12].

By using a tagged beam, we have sacrificed statistical precision for better control of systematic errors, in order to assess which previous experiments may have suffered from unrecognized systematic problems. Each systematic uncertainty summarized in Table I has been evaluated in a separate analysis, sometimes involving auxiliary measurements. The errors are, except where noted otherwise in the Table, angle-independent normalization uncertainties. The largest correction to the data and attendant uncertainty arise from cuts to remove stream 2 (but not 1 or 3) events where the np scattering vertex transverse coordinates predicted from n tagging vs p ray tracing disagree by more than 3 times the resolution σ. The removed events (6.3% of the total sample) are affected by several factors—e.g., sequential reactions in the secondary target and upstream material, or errors associated with recoil protons stopping in dead layers within the tagger—that lead to ambiguities in neutron energy and scattering angle. Combining all effects in Table I and summing uncertainties in quadrature, the net correction ($\prod c_i$) applied to raw cross sections is $\approx 1.10 \pm 0.015$, with an angle dependence of the systematic uncertainty indicated by the shaded band in Fig. 4.

The present results are in quite good absolute agreement with the Nijmegen PWA93 calculations, over the full angular range covered. The small deviations seen might be removed by minor tuning of phase shifts. In contrast, the present results deviate systematically, especially in the steepness of the back-angle cross section rise, from earlier measurements [2,3] that the Nijmegen group had rejected in their analyses by applying controversial criteria. These deviations are larger than the differences expected from the neutron energy changes among the various experiments. As the back-angle rise is particularly influential in pole extrapolations used [8,13] to extract the pion-nucleon-nucleon coupling constant, the present data strongly favor the value ($f_c^2 = 0.0748 \pm 0.0003$) given by the Nijmegen [6] and other [5] partial-wave analyses.

We thank the operations staff of the Indiana University Cyclotron Facility for providing the superior quality cooled beams, and Hal Spinka and Catherine Lechanoine-Leluc for the loan of detector hardware critical for successful execution of this experiment. We acknowledge the support of the U.S. National Science Foundation under grant no. NSF-PHY-9602872 and no. NSF-PHY-0100348.

*Present address: Department of Radiology and Radiological Sciences, Vanderbilt University, Nashville, TN, USA
†Present address: Department of Physics, University of Zagreb, Zagreb, Croatia

[1] B. E. Bonner *et al.*, Phys. Rev. Lett. **41**, 1200 (1978).
[2] J. Franz *et al.*, Phys. Scr. **T87**, 14 (2000).
[3] J. Rahm *et al.*, Phys. Rev. C **57**, 1077 (1998).
[4] V. Stoks *et al.*, Phys. Rev. C **48**, 792 (1993).
[5] D. V. Bugg and R. Machleidt, Phys. Rev. C **52**, 1203 (1995).
[6] M. C. M. Rentmeester, R. G. E. Timmermans and J. J. de Swart, Phys. Rev. C**64**, 034004 (2001).
[7] M. C. M. Rentmeester *et al.*, Phys. Rev. Lett. **81**, 5253 (1998); T. E. O. Ericson *et al.*, *ibid.* **81**, 5254 (1998).
[8] *Proceedings of Workshop on Critical Issues in the Determination of the Pion-Nucleon Coupling Constant*, edited by J. Blomgren [Phys. Scr. T87 (2000)].
[9] J. J. de Swart and R. G. E. Timmermans, Phys. Rev. C **66**, 064002 (2002).
[10] T. Peterson *et al.*, Nucl. Instrum. Methods Phys. Res., Sect. A **527**, 432 (2004).
[11] R. E. Pollock, Annu. Rev. Nucl. Part. Sci. **41**, 357 (1991).
[12] http://nn-online.org/NN/
[13] T. E. O. Ericson *et al.*, Phys. Rev. Lett. **75**, 1046 (1995).